

The Role of Diabatic Processes in Driving Ocean Heat Content Changes

Confirmation Report for
PhD in Climate Sciences
by
Maurice F. Huguenin

at the Climate Change Research Centre, UNSW Sydney

Supervisors:

Dr. Ryan M. Holmes - ryan.holmes@unsw.edu.au

Prof. Dr. Matthew H. England - m.england@unsw.edu.au

28th April 2020

Abstract

Uptake and redistribution of heat by the ocean plays a critical role in modulating the Earth's climate system. Heat content changes arise from two thermodynamic processes: *diabatic* surface forcing and vertical mixing alter a water parcel's temperature/heat content and their across-isotherm impact can lead to long-term heat uptake. *Adiabatic* transport along isotherms on the other hand is a more reversible process. On the interannual time scale, the El Niño-Southern Oscillation (ENSO) dominates heat content changes in the equatorial upper ocean. Heat absorption and release during ENSO events is strongly linked to asymmetries in the diabatic processes. On the decadal time scale, the diabatic processes play an integral part in changing anthropogenic heat anomalies. Despite the insight of new studies, our knowledge is strongly constrained by the sparse observational record and difficulties in isolating the impact of the diabatic mechanisms. In this PhD research project, we investigate recent heat content changes in a global ocean model with the water mass transformation framework that allows us to isolate surface forcing and vertical mixing. We first investigate their variability in the form of warm water volume changes during ENSO event. Next, we evaluate the role of the ocean basins in heat uptake over the recent observational record and focus on interior heat pathways between the tropics and higher latitudes. We then investigate the impact of internal climate variability on heat content changes in the Antarctic shelf region, implied basal melting of ice shelves and associated sea level rise.

Contents

Abstract	i
1 An Overview	1
2 Project I: Diabatic Contributions to Warm Water Volume Variability over ENSO Events (Completed)	2
2.1 Introduction	2
2.2 Model, Data and the WWV Budget	3
2.3 Results	5
2.4 Discussion	7
3 Project II: Basin-wide Decomposition of Anthropogenic Ocean Heat Content (Proposed)	8
3.1 Introduction	8
3.2 Model, Data and a new Spin-Up	9
3.3 Experimental Design	11
4 Project III: Climatic drivers of Variability in Antarctic Shelf Water Temperatures (Proposed)	12
4.1 Introduction	12
4.2 Model and Data	14
4.3 Experimental Design	14
5 Resource Requirements	16
6 Timeline	17

1 An Overview

Changes in the ocean's heat content (OHC) originate either from internal climate variability or external forcing (e.g. [IPCC, 2019](#), [Roemmich and Gilson, 2011](#)). Important internally-sourced drivers include the El Niño-Southern Oscillation (ENSO, [Timmermann et al., 2018](#)) and the Southern Annular Mode (SAM, [Hall and Visbeck, 2002](#)). External forcing includes anthropogenic climate change, orbital and solar variations and volcanic eruptions ([Kaufmann et al., 2011](#)). Over recent decades, the anthropogenic impact on the climate system has led to the uptake of a vast amount of energy/heat in the ocean, but many questions remain unknown due to uncertainties in the short observational record. By using numerical climate models, we are able to run focused experiments that isolate physical processes contributing to OHC changes, which is not possible with observations. The following sections present three model-based research projects (one completed and two proposed) that investigate processes driving OHC changes from the regional to the global and from the interannual to the decadal scale:

Project I focuses on the natural variability of the diabatic processes in the eastern equatorial Pacific, a key region of global ocean heat uptake. This project reconciles contradicting statements in previous studies investigating equatorial heat content changes, which are an important part of ENSO forecasting.

Project II investigates the role of different basins in recent heat uptake and large-scale redistribution. This project will help clarify where in the ocean the additional heat has been taken up, and more importantly where it has been stored. This knowledge is key in assessing future changes in sea level, ocean biogeochemistry and marine ecology.

Project III analyses the impact of tropical and midlatitude internal climate variability (ENSO and SAM) on ocean heat changes near the Antarctic shelf region and implied basal melting of sea ice from below. This project will help us better predict where the buttressing of ice shelves may become unstable in the future.

2 Project I: Diabatic Contributions to Warm Water Volume Variability over ENSO Events

The results of this project together with a discussion of the climatological warm water volume and an analysis of idealised El Niño and La Niña events stemming from my Master’s thesis are now under review for a publication in Journal of Climate. The idealised simulations are based on symmetric atmospheric forcing and further helped expose the role of ocean-sourced asymmetries in the warm water volume budget.

2.1 Introduction

The equatorial Pacific Warm Water Volume (WWV, defined as the volume of water above the 20°C isotherm in the equatorial region 120°E–80°W and 5°N–5°S, Fig. 1) is a key predictor for ENSO as it leads El Niño and La Niña events by 6–8 months (Bosc and Delcroix, 2008, McPhaden, 2012, Neske and McGregor, 2018). Since its introduction by Meinen and McPhaden (2000), it has now become an important inclusion in many analyses, models and statistical forecast schemes for ENSO (e.g. Izumo et al., 2018, Timmermann et al., 2018). However, our knowledge of the precise mechanisms influencing WWV, especially the role of diabatic processes, still remains limited. Most studies so far calculate either vertical (and in modelling studies numerical) mixing or both surface forcing and vertical mixing as the residual of the WWV budget. Consequently, this increases errors in the closure of the budget which lead to contradicting statements in several studies.

While Clarke et al. (2007), Meinen and McPhaden (2000) and Lengaigne et al. (2012) agree that diabatic processes are important contributors to WWV changes, the observation-based study by Bosc and Delcroix (2008) and the modelling study by Brown and Fedorov (2010) suggest that diabatic volume changes on ENSO-related time scales

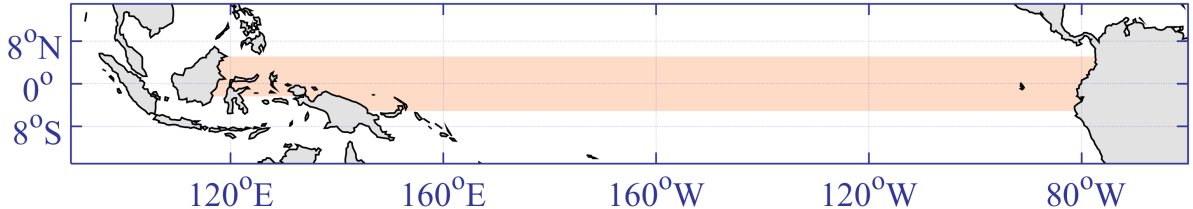


Figure 1: The Warm Water Volume (WWV) region in the equatorial Pacific 5°N and 5°S with the Indonesian Throughflow (ITF) at 2°S between the islands of Borneo and New Guinea.

are negligible, thus highlighting the importance for further analyses with other models and data sets. [Lengaigne et al. \(2012\)](#) further suggests that diabatic fluxes may also explain some of the asymmetries and non-linearities in ENSO’s underlying dynamics. In this project, we revisit the WWV budget using the water mass transformation (WMT) framework with precise online diagnostics to individually calculate each budget term during a 1979–2016 hindcast simulation and show that diabatic processes are important, and even more so during La Niña than El Niño.

2.2 Model, Data and the WWV Budget

Model and Data

In this project, we use a global ocean-sea ice model ([Kiss et al., 2019](#)) based on GFDL’s CM2.5 coupled climate model ([Delworth et al., 2012](#), [Griffies, 2012](#)) in the $1/4^{\circ}$ configuration with $50 z^*$ vertical levels. Atmospheric forcing for the model is derived from a prescribed atmospheric state using the Japanese Reanalysis product (JRA55-do, [Tsunjino et al., 2018](#)) to calculate zonal and meridional wind stress, and surface heat and freshwater fluxes using bulk formulae ([Fairall et al., 1996](#)). Vertical diffusion is parameterised using the K-profile parameterisation scheme (KPP, [Large et al., 1994](#)) and the model is eddy-resolving in the tropics. There is no explicit horizontal diffusion of tracer gradients and thus sharp lateral tracer gradients are smoothed by the numerical advection scheme. The associated diffusion is termed ‘numerical mixing’ as discussed further in [Holmes et al. \(2019\)](#). More information and discussion on the model details,

diffusive mixing parameterisations and the model performance can be found in [Spence et al. \(2017\)](#), [Stewart et al. \(2017\)](#), [Holmes et al. \(2019\)](#) and [Kiss et al. \(2019\)](#).

The Warm Water Volume Budget

To investigate the role of the diabatic heat and volume fluxes across the 20°C isotherm over ENSO, we establish the WWV budget as

$$\frac{dWWV}{dt} = \underbrace{\mathcal{T}_{5^{\circ}N+5^{\circ}S} + \mathcal{T}_{ITF} + P - E + R}_{\text{adiabatic fluxes}} + \underbrace{\mathcal{G}_F + \mathcal{G}_M + \mathcal{G}_E + \mathcal{G}_I}_{\text{diabatic fluxes}}, \quad [\text{m}^3 \text{s}^{-1}] \quad (1)$$

where $dWWV/dt$ is the WWV tendency. The adiabatic processes include the lateral transport of water masses above 20°C into and out of the WWV region across 5°N, 5°S ($\mathcal{T}_{5^{\circ}N+5^{\circ}S}$) and the Indonesian Throughflow (\mathcal{T}_{ITF}) as well as surface volume fluxes above 20°C caused by precipitation, evaporation and river runoff ($P - E + R$).

The diabatic terms include the volume fluxes across the 20°C isotherm associated with the water mass transformation of surface forcing (\mathcal{G}_F), vertical mixing (\mathcal{G}_M), eddy mixing (\mathcal{G}_E) as well as numerical mixing (\mathcal{G}_I). The surface forcing volume flux \mathcal{G}_F is driven by the surface heat flux and its different components (short-wave, long-wave, sensible and latent heat fluxes). \mathcal{G}_M is the WMT volume flux arising from parameterised diffusive vertical mixing processes. Through heating and cooling fluid, diffusive mixing likewise moves water across temperatures classes. These two WMT fluxes depend on the across-isotherm heat fluxes as discussed in detail in the manuscript ([Huguenin et al., 2020a](#)). Additionally, the budget includes terms associated with the parameterisation of submesoscale ([Fox-Kemper et al., 2008](#)) and mesoscale eddies ([Gent and McWilliams, 1990](#), [Redi, 1982](#)). These fluxes make negligible contributions to the WWV budget but are included in our calculation as \mathcal{G}_E (eddy mixing) in order to accurately calculate numerical mixing as the residual. Numerical mixing \mathcal{G}_I arises from numerical diffusion associated with truncation errors in the model's tracer advection scheme.

2.3 Results

Before discussing the role of diabatic processes in discharging and recharging of heat during El Niño and La Niña events, we first take a look at their spatial distribution during September-November, when their seasonal cycle peaks. Both diabatic processes are focused in the eastern equatorial Pacific. There, surface forcing is consistently warming the surface region (red region, Fig. 2a). Vertical mixing on the other hand cools surface water masses and simultaneously warms deeper layers, represented by the negative (blue) and positive (red) across-isotherm (or diathermal) velocity regions in Fig. 2b. The 20°C isotherm is positioned on average in the warming region of both diabatic fluxes, indicating a net upward volume flux across the isotherm into the WWV above.

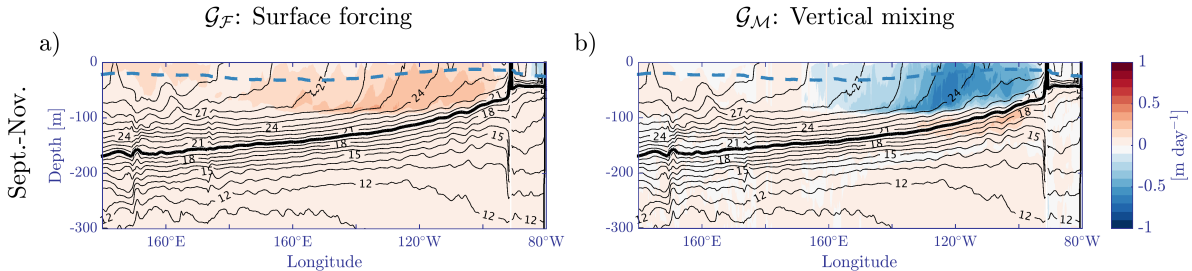


Figure 2: Equatorial Pacific transects of the simulated climatological (a) surface forcing and (b) vertical mixing water mass transformation velocities [m day^{-1}] for boreal autumn (SON). Surface forcing warms upper layers, increasing their volume and inducing a volume flux across the 20°C isotherm. Vertical mixing cools surface and warms subsurface waters, leading to across-isotherm volume exchanges. The discontinuity at 90°W is caused by the model's bathymetry near the Galápagos Islands.

During El Niño and La Niña events, both diabatic processes undergo stark contrasting and asymmetric changes. Weaker trade winds during El Niño reduce upwelling of cold water, moving the 20°C isotherm away from the surface while also increasing eastern equatorial SSTs and driving an anomalous surface heat flux into the atmosphere. This results in an anomalous discharge of WWV due to surface forcing (dark blue line during red El Niño periods, Fig. 3). At the same time, the deepening 20°C isotherm moves away from the region of strong wind- and shear-driven mixing, whose intensity also reduces (Fig. 4a).

During La Niña, the stronger trade winds increase upwelling of cold water masses

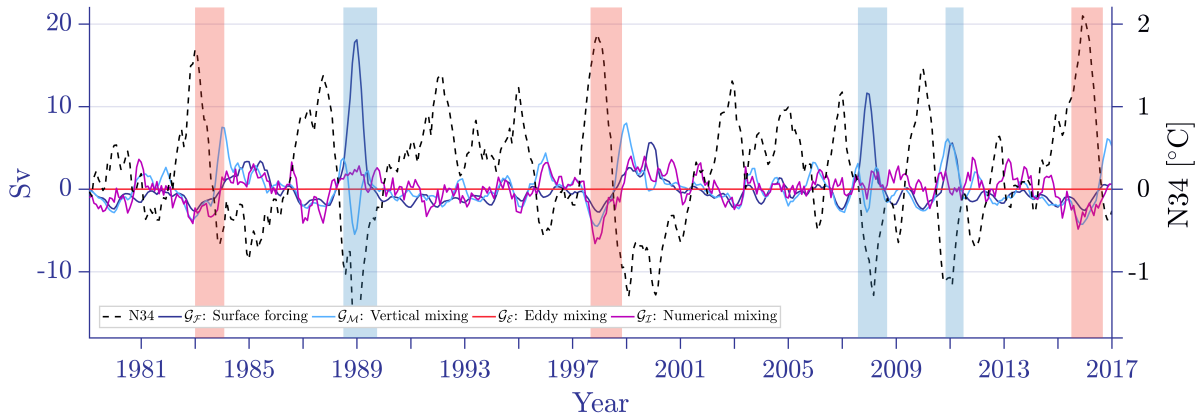


Figure 3: Time series of the diabatic WWV budget terms [Sv] in the 1979-2016 hindcast simulation. The Niño 3.4 index [$^{\circ}\text{C}$] (N34, defined as the sea surface temperature anomaly in the region 170°W - 120°W and 5°N - 5°S) is given as a dashed line. The shading in red and blue shows the WWV discharge and recharge periods during three strong El Niño and La Niña events each.

and the 20°C isotherm shoals, sometimes outcropping in the eastern Pacific. Exposure of the 20°C isotherm to increased heat uptake by surface forcing in this region creates a strong across-isotherm volume flux responsible for most of the WWV recharge (dark blue line during blue La Niña periods, Fig. 3). While turbulence is enhanced during La Niña, the shoaling of the isotherm into the surface layers means that vertical mixing can drive an anomalous discharge of WWV (Fig. 4d). This key asymmetry, that mixing drives anomalous discharge in both El Niño and La Niña events (see light blue time series during the red and blue shaded periods in Fig. 3), arises from the strong dependence of the diabatic fluxes on the position of the 20°C isotherm. However, the contribution of vertical mixing to the overall discharge during La Niña is concealed by opposing volume fluxes occurring at different times as the 20°C isotherm transitions through regions of vertical mixing-driven warming and cooling. On average, the ratio of the diabatic to adiabatic contributions to WWV changes during El Niño is about 40%:60% while for La Niña, this ratio changes to 75%:25%.

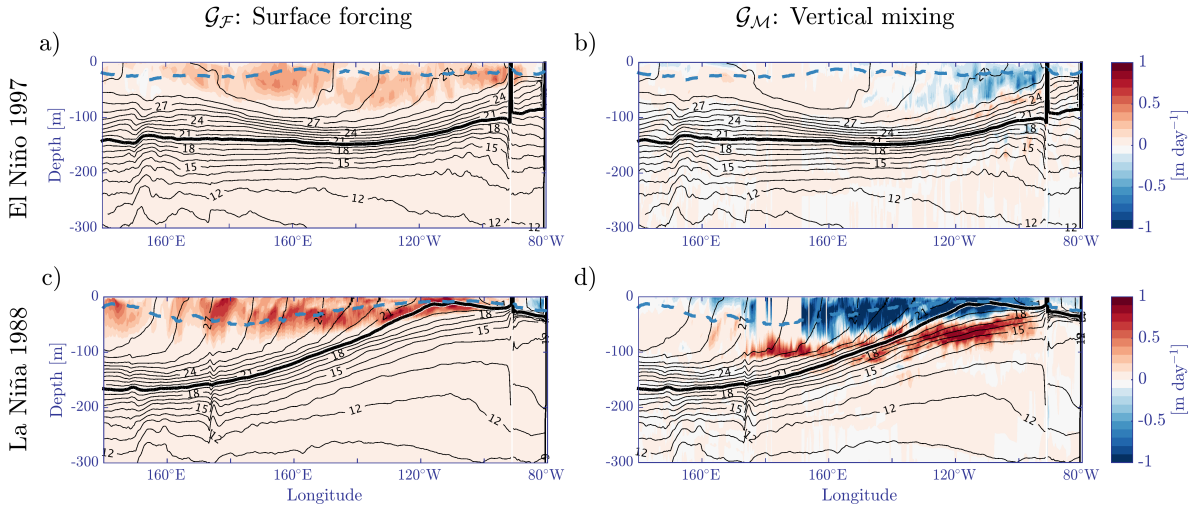


Figure 4: Equatorial Pacific transects of the surface forcing and vertical mixing water mass transformation velocities [m day^{-1}] for boreal autumn (SON) during El Niño 1997 and La Niña 1988. The 20°C isotherm is highlighted in bold and the mixed layer depth is the dashed light blue line. Surface forcing warms upper layers, increases their volume and induces a volume flux across the 20°C isotherm. Vertical mixing cools surface and warms subsurface waters, leading to across-isotherm volume exchanges.

2.4 Discussion

While the diabatic fluxes in the observed WWV budget in [Meinen and McPhaden \(2000\)](#) could only be derived as the residual from horizontal transport, the model study by [Brown and Fedorov \(2010\)](#) showed that errors in the calculation of horizontal fluxes can be of the same magnitude as the vertical (diabatic) fluxes. They further present evidence that the vertical fluxes on ENSO-related time scales in the eastern Pacific are small, contradicting [Meinen and McPhaden \(2000\)](#) and [Lengaigne et al. \(2012\)](#). By revisiting the WWV budget here with a precise online calculation of the individual terms, we are able to further minimise errors associated with the budget closure and highlight the dominant role of the diabatic fluxes during La Niña. Despite differences to [Meinen and McPhaden \(2000\)](#) and [Lengaigne et al. \(2012\)](#) in the methods used to calculate the budget terms (limited observations vs. the use of different models, parameterisations and atmospheric forcing), our study supports their main finding that the diabatic and adiabatic volume fluxes are equally important in driving WWV changes on ENSO time scales. Moreover, we highlight the key role of the equatorial Pacific in vertical heat exchanges, which might play an important part in anthropogenic heat uptake.

3 Project II: Basin-wide Decomposition of Anthropogenic Ocean Heat Content

3.1 Introduction

Since 1955, the global ocean has taken up an additional $24 \pm 1.9 \times 10^{22}$ Joules of heat, accounting for an uptake of more than 93% of the additional anthropogenic energy in the Earth's climate system (IPCC, 2013, Levitus et al., 2012, Meyssignac et al., 2019). Over the last 30 years, it is likely that the rate of warming in the oceans has even doubled (IPCC, 2019). Observational and model studies (e.g. Cai et al., 2010, Frölicher et al., 2015, Liu et al., 2018, Purkey et al., 2019) suggest that the Southern Ocean dominates anthropogenic heat uptake. In the North Atlantic, anthropogenic heat uptake is currently suppressed by the high concentration of anthropogenic aerosols cooling the regional climate and offsetting the strong surface heat fluxes (Irving et al., 2019, Shi et al., 2018a). Future projections however show that the North Atlantic is likely to play a more dominant role in anthropogenic heat uptake (Shi et al., 2018a). Many studies have investigated the role of individual ocean basins in modulating anthropogenic climate change (e.g. Gregory et al., 2016, Shi et al., 2018b), however the role of large-scale oceanic heat redistribution still remains relatively unknown. This is not least because of the short observational period, sparse data coverage (especially in the Southern Ocean) and difficulties in measuring the small variations relative to the global inventory (Meyssignac et al., 2019). Additionally, the internal variability of the climate system is redistributing heat within and across basin, and can mask the observed anthropogenic signal (England et al., 2014). In this research project, our focus will be on isolating the forced anthropogenic heat signals and evaluate the relative importance of the local/regional and large-scale dynamical processes in heat uptake and redistribution.

3.2 Model, Data and a new Spin-Up

As in Project I, we will be using the global ocean sea-ice model from [Kiss et al. \(2019\)](#), introduced in Section 2.2. The spin-up approach used in Project I with five repeat cycles of JRA55-do forcing simulates the upper ocean WWV changes reasonably well compared to observations (Fig. 9 in [Huguenin et al., 2020a](#)), but underestimates global ocean heat content (Fig. 5). This could be caused by the way the model has been equilibrated with five repeat cycles. For this project, we aim for well-equilibrated pre-industrial conditions in the model before applying anthropogenic forcing. We propose a repeat-decade approach that includes applying 10-year cycles of 1963–1972 JRA55-do forcing for 300 years. Compared to a true pre-industrial spin-up (e.g. a decade before the 1850s), we choose this more recent period as only good forcing data from 1958 onwards is available and this decade occurs before the significant 1°C warming trend that began around 1980 (Fig. 6a). The significant linear surface air temperature (SAT) trend in this decade will not be an issue as it will be evened out over the 300-year spin-up. The 1963–1972 decade, compared to the ones five years earlier/later, has weaker spatial SAT anomalies in the North Atlantic and close to neutral conditions in the Interdecadal Pacific Oscillation (cf. panels a-c in Fig. 6). A first preliminary run will be performed with the 1° configuration before using the higher resolution versions. We may also examine alternate baseline decades or multi-decade simulations with the Coordinated Ocean-ice Reference Experiment interannual forcing product (CORE-IAF, [Large and Yeager, 2004](#)) for a spin-up if observations are not well-reproduced by the model.

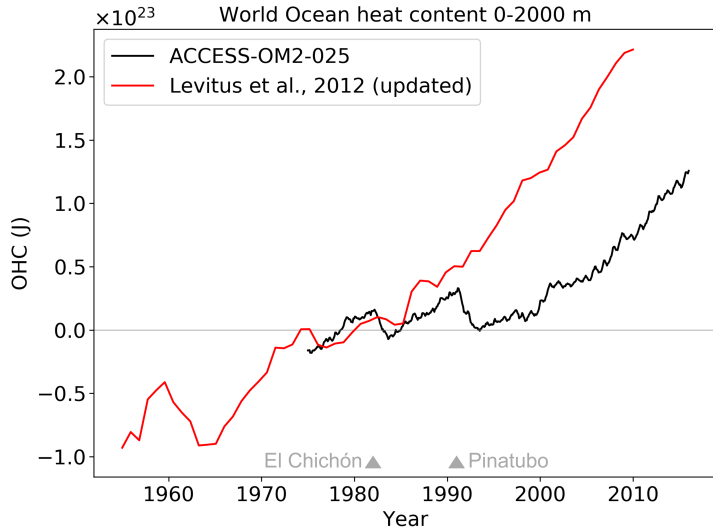


Figure 5: Time series of the observed (red) and modelled (black) estimate of global ocean heat uptake (Levitus et al., 2012). ACCESS-OM2 is the acronym for the Kiss et al. (2019) global ocean-sea ice model we use in all three projects. The large difference between observed and simulated OHC likely arises from the spin-up adopting five cycles of 1958–2018 forcing, when anthropogenic warming was already underway. A 5-year moving average has been applied in Levitus et al. (2012) while the simulated time series shows monthly mean data.

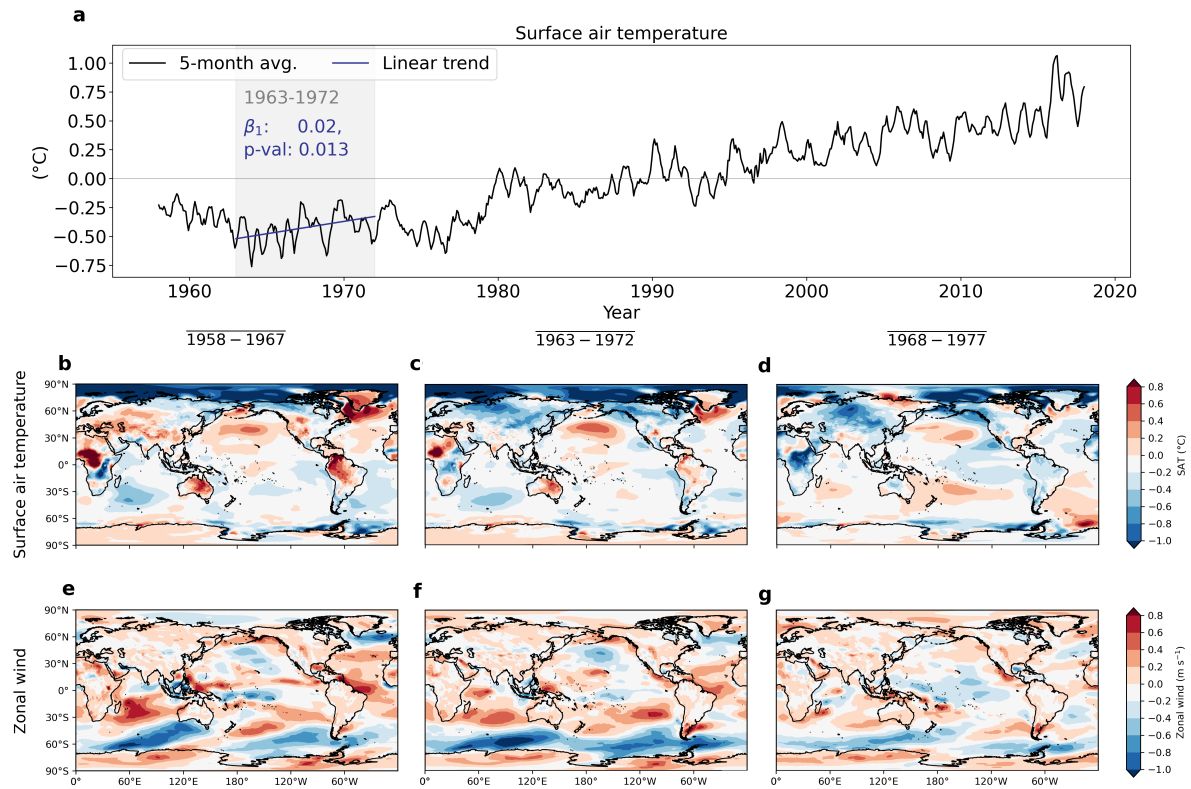


Figure 6: In (a) the time series of anomalous global surface air temperature ($^{\circ}\text{C}$) in the JRA55-do reanalysis. In grey the 1963–1972 decade chosen for the repeat-decade forcing spin-up and in blue the significant trend which will be evened out over the 300-year simulation. In (b, c, d) the spatial distribution of anomalous mean surface air temperature and in (e, f, g) of zonal wind (m s^{-1}) in the JRA55-do reanalysis during 1958–1967, 1963–1972 and 1968–1977.

3.3 Experimental Design

As a first step, we will complete the new spin-up followed by a control simulation:

- Spin-up 300-year repeat decade forcing (RDF) using JRA55-do for 1963–1972
- EXP_{CTRL} 60-year control simulation with RDF following the spin-up. Anomalies in the perturbation experiments will then be evaluated relative to this simulation to account for model drift.

To investigate the role of the tropics, the mid- and high latitudes in anthropogenic heat uptake and interior transport, we propose to undertake the following perturbation experiments initialised from EXP_{CTRL} :

- $\text{EXP}_{\text{TROPICS}}$ As in EXP_{CTRL} but with interannual forcing (IAF) of 1960–2020 over the tropics (25°S – 25°N)
- $\text{EXP}_{\text{MID-LAT}}$ As in EXP_{CTRL} but with IAF over the midlatitudes (25° – 60°N/S)
- $\text{EXP}_{\text{POLAR}}$ As in EXP_{CTRL} but with IAF over the polar latitude ($\geq 60^{\circ}\text{N/S}$)

To decompose the anthropogenic heat uptake by basins, we additionally propose:

- EXP_{IP} As in EXP_{CTRL} but with IAF over the Indo-Pacific north of 40°S
- EXP_{SO} As in EXP_{CTRL} but with IAF over the Southern Ocean south of 40°S
- EXP_{AO} As in EXP_{CTRL} but with IAF over the Atlantic Ocean north of 40°S

The analysis in these runs will focus on heat uptake and heat content/residual trends and evaluate the relative contribution of the adiabatic and diabatic processes (similar to Project I). The WMT diagnostics allow us to analyse these simulations with respect to interior heat transport in temperature space (i.e. the latitude/depth vs. temperature plane). We expect that vertical mixing and its components may play a major role in the transport of the anthropogenic residual from uptake regions to storage predominantly in the Southern Ocean.

4 Project III: Climatic drivers of Variability in Antarctic Shelf Water Temperatures

4.1 Introduction

Over recent decades, melting of the Antarctic ice sheet has accelerated, directly resulting in increased sea level rise. Most of the mass loss occurs through basal melting when warm, salty, subsurface circumpolar deep water (CDW) is pushed onto the Antarctic shelf and enters ice shelf cavities (Nakayama et al., 2018, Rignot et al., 2019). Episodes of CDW upwelling onto the shelf are strongly affected by surface wind stresses, which in turn are modulated by the El Niño-Southern Oscillation (ENSO) and the Southern Annular Mode (SAM, Gao et al., 2018, Holland et al., 2019).

El Niño events in the equatorial region lead to warm CDW on the Antarctic shelf through ENSO's teleconnection to the Amundsen Sea that strengthens polar westerlies (Fig. 7a, Scott Yiu and Maycock, 2019). Likewise, subsurface warming of Antarctic coastal waters is modulated through enhanced poleward shifting westerlies during positive SAM events (Fig. 7b, Jacobs, 2006, Spence et al., 2014). For both ENSO and SAM, warming is largest in the Bellingshausen and Amundsen Seas due to the close proximity between the colder shelf region and the warm CDW, and because of the steep topography west of the Antarctic Peninsula (Spence et al., 2017).

The strongest high-latitude ice-ocean response and strongest upwelling of CDW occurs during periods when ENSO and SAM events coincide (i.e. El Niño and a positive SAM, and vice versa for La Niña, Stammerjohn et al., 2008). The interactions between ENSO and SAM events and their impacts on the interannual to decadal variability of CDW on the continental shelf however remain largely unknown. In this project, we propose to run perturbation experiments in the Kiss et al. (2019) global ocean model and investigate how the large-scale atmospheric teleconnections of ENSO and SAM feed into localized circulation changes on the Antarctic shelf.

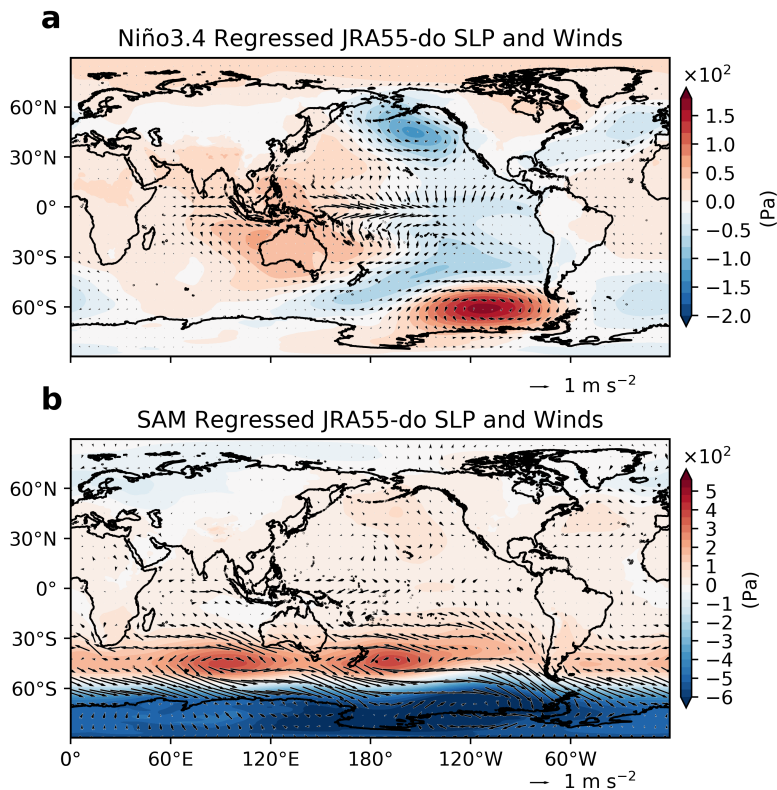


Figure 7: Regression maps of the observed (a) Niño 3.4 (Rayner et al., 2003) and (b) SAM (Gong and Wang, 1999) indices onto JRA55-do sea level pressure (Pa) and near-surface winds (m s^{-2}). Sea level pressure data is given as shading and the wind vectors are given as arrows. Notice the different scales in both panels.

4.2 Model and Data

As in Projects I and II, we will be using the Kiss et al. (2019) ocean-sea ice model in the $1/4^\circ$ and $1/10^\circ$ horizontal resolution with JRA55-do forcing. It will be important to do some of the experiments in the high resolution version with a much better resolved shelf region. Further, upwelling of CDW is strongly linked to eddy variability (Thompson et al., 2014), and the three configurations vary in their ability to simulate submeso- and mesoscale eddies. The 1° version is not resolving eddies, the $1/4^\circ$ has eddy parameterisation schemes and the $1/10^\circ$ version is eddy-resolving up to a Rossby Number $R_{crit} \simeq 2$ (about 60°S , Hallberg, 2013, Kiss et al., 2019). For more information on the model, see also Sections 2.2 and 3.2.

4.3 Experimental Design

We propose the following simulations to investigate the isolated impact of internal climate variability on ocean heat changes in the Antarctic shelf region:

Spin-up & EXP _{CTRL}	As in Project II, see Section 3.2
EXP _{ENSO-Winds}	Simulation with time-varying ENSO-related Southern Ocean wind regression pattern (see Fig. 7a for the anomalies). While El Niño increases warming of the shelf in the Pacific sector, La Niña leads to cooling and potentially to asymmetries between the two phases.
EXP _{ENSO-All}	As in EXP _{ENSO-Winds} but with ENSO perturbation anomalies in all forcing fields to additionally capture ENSO's surface air temperature and specific humidity impacts which also influence sea surface temperature and eddy variability
EXP _{SAM-Winds}	As in EXP _{ENSO-Winds} but with SAM wind regression patterns (see Fig. 7b)
EXP _{SAM-All}	As in EXP _{ENSO-All} but with SAM-related perturbation anomalies

in all forcing fields. This experiment will give us more insight into the variability of the shelf circulation in Eastern Antarctica where the interannual variability of SAM is strongest (opposed to ENSO’s strongest impact in Western Antarctica, Fig. 7b, Spence et al., 2017).

$\text{EXP}_{\text{ENSO-SAM}}$ Investigating the atmospheric impact of ENSO and SAM on the Antarctic shelf by combining $\text{EXP}_{\text{ENSO-All}}$ and $\text{EXP}_{\text{SAM-All}}$ forcing

The analysis in these runs will focus on the temporal and spatial evolution of warm water on the Antarctic shelf in the Amundsen Sea region. We expect the strongest upwelling signals in the $\text{EXP}_{\text{ENSO-Winds}}$ and $\text{EXP}_{\text{SAM-Winds}}$ simulations when El Niño co-occurs with positive SAM events. We also expect considerable residual anomalies occurring from the asymmetries in the ENSO cycle that may lead to longer-term impacts on Antarctic shelf water masses, (i.e. anomalies after the ENSO cycle of El Niño followed by La Niña).

5 Resource Requirements

The main resources required for these research projects are CPU time and storage at the NCI facility in Canberra. We will apply annually for resources as part of the NCI project ‘Past, Present and Future Climate Variability and Change in the Southern Hemisphere’ through the National Computational and Merit Allocation Scheme and propose the following values defined by Table 1:

Project II:	– 1° configuration 300-year spin-up	300 × [0.1 kSU, 2.5 GB]
	– 1° configuration 60-year IAF* run	60 × [0.1 kSU, 2.5 GB]
	– 1/4° configuration 300-year spin-up	300 × [4.5 kSU, 48 GB]
	– 1/4° configuration six 60-year IAF runs	6 × 60 × [4.5 kSU, 48 GB]
		<hr/> total : 3 MSU**, 5 TB
Project III:	– 1/4° configuration five 60-year IAF runs	5 × 60 × [4.5 kSU, 48 GB]
	– 1/10° configuration 60-year IAF runs	60 × [60 kSU, 113 GB]
		<hr/> total : 4.9 MSU, 9 TB

→ Note that we will not store all spin-up data allowing us to save substantial storage.

Table 1: Specifics for the three configurations of the Kiss et al. (2019) ocean-sea ice model used in this study. The last column indicates storage of output including WMT diagnostics.

Lateral Grid	Vertical Grid	Walltime [h/yr]	CPU time [kSU/hr]	Storage [GB/yr]
1°	50 z* levels	~0.38	0.1	2.5
0.25°	50 z* levels	2.6	4.5	48
0.1°	75 z* levels	19.9	55–65	113

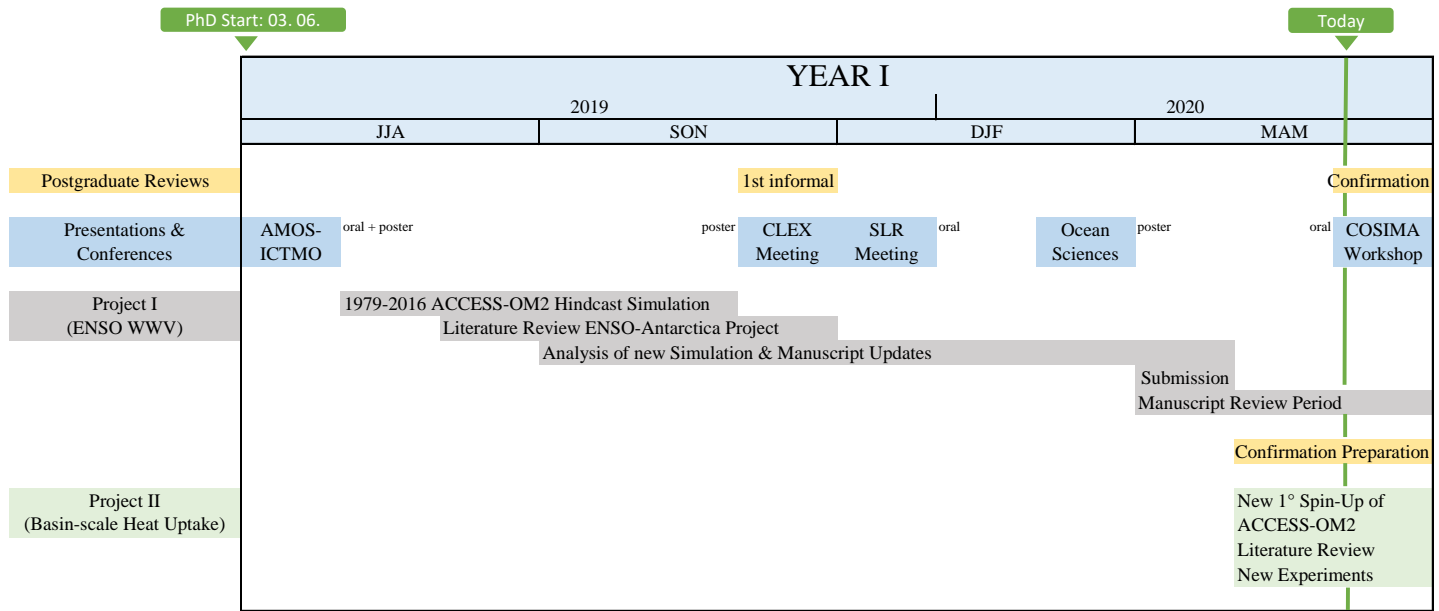
Compliance with UNSW Policies

This PhD research project will be conducted in accordance with the UNSW policies for intellectual property, occupational health and safety (OHS) and ethics: <https://research.unsw.edu.au/research-integrity-policies-and-procedures>.

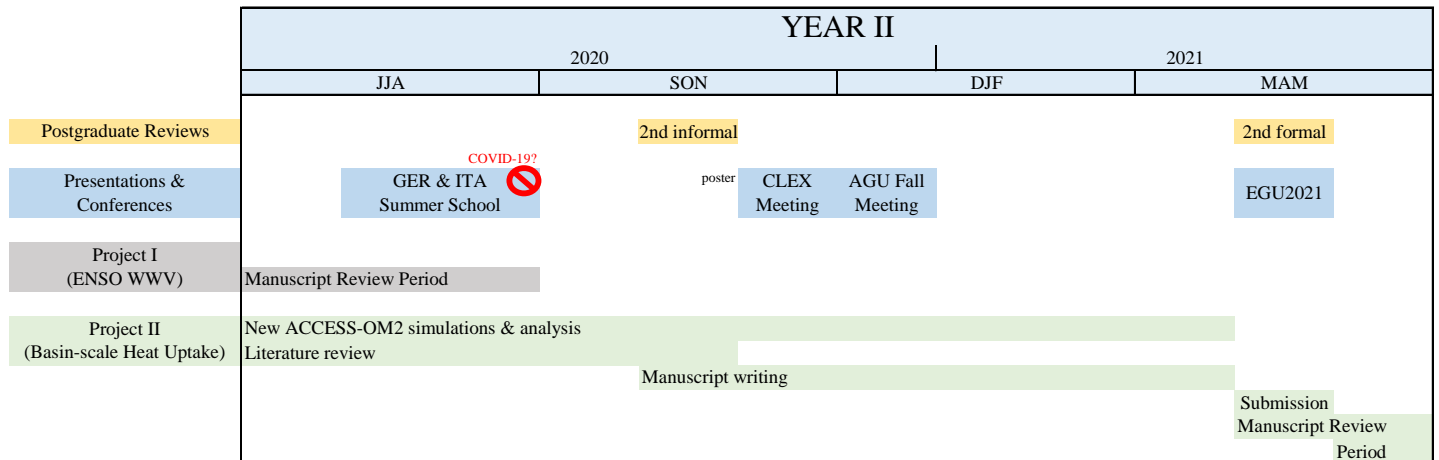
*IAF = interannually forced simulation with JRA55-do for 1958–2018

**1 MSU = 10^3 kSU = 10^6 SU; SU, a service unit, is approximately one CPU hour

6 Timeline



During this first year of my PhD, I have also dedicated time to publishing [Huguenin et al. \(2020b\)](#).



References

- Bosc, C. and Delcroix, T. Observed equatorial Rossby waves and ENSO-related warm water volume changes in the equatorial Pacific Ocean. *Journal of Geophysical Research: Oceans*, 113(C6), 2008. doi: [10.1029/2007JC004613](https://doi.org/10.1029/2007JC004613).
- Brown, J. N. and Fedorov, A. V. Estimating the Diapycnal Transport Contribution to Warm Water Volume Variations in the Tropical Pacific Ocean. *Journal of Climate*, 23(2):221–237, 2010. doi: [10.1175/2009JCLI2347.1](https://doi.org/10.1175/2009JCLI2347.1).
- Cai, W., Cowan, T., Godfrey, S., and Wijffels, S. Simulations of Processes Associated with the Fast Warming Rate of the Southern Midlatitude Ocean. *Journal of Climate*, 23(1):197–206, 2010. doi: [10.1175/2009JCLI3081.1](https://doi.org/10.1175/2009JCLI3081.1).
- Clarke, A. J., Van Gorder, S., and Colantuono, G. Wind Stress Curl and ENSO Discharge/Recharge in the Equatorial Pacific. *Journal of Physical Oceanography*, 37(4): 1077–1091, 2007. doi: [10.1175/JPO3035.1](https://doi.org/10.1175/JPO3035.1).
- Delworth, T. L., Rosati, A., Anderson, W., Adcroft, A. J., Balaji, V., Benson, R., Dixon, K., Griffies, S. M., Lee, H.-C., Pacanowski, R. C., et al. Simulated Climate and Climate Change in the GFDL CM2.5 High-Resolution Coupled Climate Model. *Journal of Climate*, 25(8):2755–2781, 2012. doi: [10.1175/JCLI-D-11-00316.1](https://doi.org/10.1175/JCLI-D-11-00316.1).
- England, M. H., McGregor, S., Spence, P., Meehl, G. A., Timmermann, A., Cai, W., Gupta, A. S., McPhaden, M. J., Purich, A., and Santoso, A. Recent intensification of wind-driven circulation in the Pacific and the ongoing warming hiatus. *Nature Climate Change*, 4(3):222–227, 2014. doi: [10.1038/NCLIMATE2106](https://doi.org/10.1038/NCLIMATE2106).
- Fairall, C. W., Bradley, E. F., Rogers, D. P., Edson, J. B., and Young, G. S. Bulk parameterization of air-sea fluxes for tropical ocean-global atmosphere coupled-ocean atmosphere response experiment. *Journal of Geophysical Research: Oceans*, 101(C2): 3747–3764, 1996. doi: [10.1029/95JC03205](https://doi.org/10.1029/95JC03205).

- Fox-Kemper, B., Danabasoglu, G., Ferrari, R., and Hallberg, R. W. Parameterizing Submesoscale Physics in Global Climate Modelse. *CLIVAR Exchanges*, 13:1317, 2008.
- Frölicher, T. L., Sarmiento, J. L., Paynter, D. J., Dunne, J. P., Krasting, J. P., and Winton, M. Dominance of the Southern Ocean in Anthropogenic Carbon and Heat Uptake in CMIP5 Models. *Journal of Climate*, 28(2):862–886, 2015. doi: [10.1175/JCLI-D-14-00117.1](https://doi.org/10.1175/JCLI-D-14-00117.1).
- Gao, L., Rintoul, S. R., and Yu, W. Recent wind-driven change in Subantarctic Mode Water and its impact on ocean heat storage. *Nature Climate Change*, 8(1):58–63, 2018. doi: [10.1038/s41558-017-0022-8](https://doi.org/10.1038/s41558-017-0022-8).
- Gent, P. R. and McWilliams, J. C. Isopycnal Mixing in Ocean Circulation Models. *Journal of Physical Oceanography*, 20(1):150–155, 1990. doi: [10.1175/1520-0485\(1990\)020j0150:IMOCM;2.0.CO;2](https://doi.org/10.1175/1520-0485(1990)020j0150:IMOCM;2.0.CO;2).
- Gong, D. and Wang, S. Definition of antarctic oscillation index. *Geophysical Research Letters*, 26(4):459–462, 1999. doi: [10.1029/1999GL900003](https://doi.org/10.1029/1999GL900003).
- Gregory, J. M., Bouttes, N., Griffies, S. M., Haak, H., Hurlin, W. J., Jungclaus, J., Kelley, M., Lee, W. G., Marshall, J., Romanou, A., Saenko, O. A., Stammer, D., and Winton, M. The Flux-Anomaly-Forced Model Intercomparison Project (FAFMIP) contribution to CMIP6: investigation of sea-level and ocean climate change in response to CO₂ forcing. *Geoscientific Model Development*, 9(11):3993–4017, 2016. doi: [10.5194/gmd-9-3993-2016](https://doi.org/10.5194/gmd-9-3993-2016).
- Griffies, S. M. Elements of the modular ocean model (MOM). *GFDL Ocean Group Tech. Rep.*, 7:620, 2012.
- Hall, A. and Visbeck, M. Synchronous Variability in the Southern Hemisphere Atmosphere, Sea Ice, and Ocean Resulting from the Annular Mode. *Journal of Climate*, 15(21):3043–3057, 2002. doi: [10.1175/1520-0442\(2002\)015j3043:SVITSH;2.0.CO;2](https://doi.org/10.1175/1520-0442(2002)015j3043:SVITSH;2.0.CO;2).

Hallberg, R. Using a resolution function to regulate parameterizations of oceanic mesoscale eddy effects. *Ocean Modelling*, 72:92 – 103, 2013. doi: [10.1016/j.ocemod.2013.08.007](https://doi.org/10.1016/j.ocemod.2013.08.007).

Holland, P. R., Bracegirdle, T. J., Dutrieux, P., Jenkins, A., and Steig, E. J. West Antarctic ice loss influenced by internal climate variability and anthropogenic forcing. *Nature Geoscience*, 12(9):718–724, 2019. doi: [10.1038/s41561-019-0420-9](https://doi.org/10.1038/s41561-019-0420-9).

Holmes, R. M., Zika, J. D., and England, M. H. Diathermal Heat Transport in a Global Ocean Model. *Journal of Physical Oceanography*, 49(1):141–161, 2019. doi: [10.1175/JPO-D-18-0098.1](https://doi.org/10.1175/JPO-D-18-0098.1).

Huguenin, M. F., Holmes, R. M., and England, M. H. Diabatic Contributions to Warm Water Volume Variability Over ENSO Events. *Journal of Climate*, 2020a. In Review.

Huguenin, M. F., Fischer, E. M., Kotlarski, S., Scherrer, S. C., Schwierz, C., and Knutti, R. Lack of Change in the Projected Frequency and Persistence of Atmospheric Circulation Types Over Central Europe. *Geophysical Research Letters*, 2020b. doi: [10.1029/2019GL086132](https://doi.org/10.1029/2019GL086132).

IPCC. Summary for Policymakers. In *Climate Change 2013: The Physical Science Basis. Contribution of Working Group I to the Fifth Assessment Report of the Intergovernmental Panel on Climate Change [Stocker, T.F., D. Qin, G.-K. Plattner, M. Tignor, S.K. Allen, J. Boschung, A. Nauels, Y. Xia, V. Bex and P.M. Midgley (eds.)]*. Cambridge University Press, Cambridge, United Kingdom and New York, NY, USA, 2013.

IPCC. Summary for Policymakers. In *IPCC Special Report on the Ocean and Cryosphere in a Changing Climate [H.-O. Pörtner, D.C. Roberts, V. Masson-Delmonte, P. Zhai, M. Tignor, E. Poloczanska, K. Mintenbeck, M. Nicolai, A. Okem, J. Petzold, B. Rama, N. Weyer (eds.)]*. In press., 2019.

Irving, D. B., Wijffels, S., and Church, J. A. Anthropogenic Aerosols, Greenhouse

- Gases, and the Uptake, Transport, and Storage of Excess Heat in the Climate System. *Geophysical Research Letters*, 46(9):4894–4903, 2019. doi: [10.1029/2019GL082015](https://doi.org/10.1029/2019GL082015).
- Izumo, T., Lengaigne, M., Vialard, J., Suresh, I., and Planton, Y. On the physical interpretation of the lead relation between Warm Water Volume and the El Niño Southern Oscillation. *Climate Dynamics*, pages 1–20, 2018. doi: [10.1007/s00382-018-4313-1](https://doi.org/10.1007/s00382-018-4313-1).
- Jacobs, S. Observations of change in the Southern Ocean. *Philosophical Transactions of the Royal Society A: Mathematical, Physical and Engineering Sciences*, 364(1844): 1657–1681, 2006. doi: [10.1098/rsta.2006.1794](https://doi.org/10.1098/rsta.2006.1794).
- Kaufmann, R. K., Kauppi, H., Mann, M. L., and Stock, J. H. Reconciling anthropogenic climate change with observed temperature 1998–2008. *Proceedings of the National Academy of Sciences*, 108(29):11790–11793, 2011. doi: [10.1073/pnas.1102467108](https://doi.org/10.1073/pnas.1102467108).
- Kiss, A. E., Hogg, A. M., Hannah, N., Boeira Dias, F., Brassington, G. B., Chamberlain, M. A., Chapman, C., Dobrohotoff, P., Domingues, C. M., Duran, E. R., England, M. H., Fiedler, R., Griffies, S. M., Heerdegen, A., Heil, P., Holmes, R. M., Klocker, A., Marsland, S. J., Morrison, A. K., Munroe, J., Oke, P. R., Nikurashin, M., Pilo, G. S., Richet, O., Savita, A., Spence, P., Stewart, K. D., Ward, M. L., Wu, F., and Zhang, X. ACCESS-OM2: A Global Ocean-Sea Ice Model at Three Resolutions. *Geoscientific Model Development Discussions*, 2019:1–58, 2019. doi: [10.5194/gmd-2019-106](https://doi.org/10.5194/gmd-2019-106).
- Large, W. G., McWilliams, J. C., and Doney, S. C. Oceanic vertical mixing: A review and a model with a non-local boundary layer parameterization. *Reviews of Geophysics*, 32(4):363–403, 1994. doi: [10.1029/94rg01872](https://doi.org/10.1029/94rg01872).
- Large, W. G. and Yeager, S. G. Diurnal to Decadal Global Forcing for Ocean and Sea-Ice Models: The Data Sets and Flux Climatologies. *NCAR Technical Note*, 2004. doi: [10.5065/D6KK98Q6](https://doi.org/10.5065/D6KK98Q6).

- Lengaigne, M., Hausmann, U., Madec, G., Menkes, C., Vialard, J., and Molines, J.-M. Mechanisms controlling warm water volume interannual variations in the equatorial Pacific: Diabatic versus adiabatic processes. *Climate Dynamics*, 38(5-6):1031–1046, 2012. doi: [10.1007/s00382-011-1051-z](https://doi.org/10.1007/s00382-011-1051-z).
- Levitus, S., Antonov, J. I., Boyer, T. P., Baranova, O. K., Garcia, H. E., Locarnini, R. A., Mishonov, A. V., Reagan, J. R., Seidov, D., Yarosh, E. S., and Zweng, M. M. World ocean heat content and thermosteric sea level change (02000 m), 19552010. *Geophysical Research Letters*, 39(10), 2012. doi: [10.1029/2012GL051106](https://doi.org/10.1029/2012GL051106).
- Liu, W., Lu, J., Xie, S.-P., and Fedorov, A. Southern Ocean Heat Uptake, Redistribution, and Storage in a Warming Climate: The Role of Meridional Overturning Circulation. *Journal of Climate*, 31(12):4727–4743, 2018. doi: [10.1175/JCLI-D-17-0761.1](https://doi.org/10.1175/JCLI-D-17-0761.1).
- McPhaden, M. J. A 21st century shift in the relationship between ENSO SST and warm water volume anomalies. *Geophysical Research Letters*, 39(9), 2012. doi: [10.1029/2012GL051826](https://doi.org/10.1029/2012GL051826).
- Meinen, C. S. and McPhaden, M. J. Observations of Warm Water Volume Changes in the Equatorial Pacific and their Relationship to El Niño and La Niña. *Journal of Climate*, 13(20):3551–3559, 2000. doi: [10.1175/1520-0442\(2000\)013;3551:OOWWVC;2.0.CO;2](https://doi.org/10.1175/1520-0442(2000)013;3551:OOWWVC;2.0.CO;2).
- Meyssignac, B., Boyer, T., Zhao, Z., Hakuba, M. Z., Landerer, F. W., Stammer, D., Khl, A., Kato, S., LEcuyer, T., Ablain, M., Abraham, J. P., Blazquez, A., Cazenave, A., Church, J. A., Cowley, R., Cheng, L., Domingues, C. M., Giglio, D., Gouretski, V., Ishii, M., Johnson, G. C., Killick, R. E., Legler, D., Llovel, W., Lyman, J., Palmer, M. D., Piotrowicz, S., Purkey, S. G., Roemmich, D., Roca, R., Savita, A., Schuckmann, K. v., Speich, S., Stephens, G., Wang, G., Wijffels, S. E., and Zilberman, N. Measuring Global Ocean Heat Content to Estimate the Earth Energy Imbalance. *Frontiers in Marine Science*, 6:432, 2019. doi: [10.3389/fmars.2019.00432](https://doi.org/10.3389/fmars.2019.00432).

Nakayama, Y., Menemenlis, D., Zhang, H., Schodlok, M., and Rignot, E. Origin of Circumpolar Deep Water intruding onto the Amundsen and Bellingshausen Sea continental shelves. *Nature Communications*, 9(1):3403, 2018. doi: [10.1038/s41467-018-05813-1](https://doi.org/10.1038/s41467-018-05813-1).

Neske, S. and McGregor, S. Understanding the warm water volume precursor of ENSO events and its interdecadal variation. *Geophysical Research Letters*, 45(3):1577–1585, 2018. doi: [10.1002/2017GL076439](https://doi.org/10.1002/2017GL076439).

Purkey, S. G., Johnson, G. C., Talley, L. D., Sloyan, B. M., Wijffels, S. E., Smethie, W., Mecking, S., and Katsumata, K. Unabated Bottom Water Warming and Freshening in the South Pacific Ocean. *Journal of Geophysical Research: Oceans*, 124(3):1778–1794, 2019. doi: [10.1029/2018JC014775](https://doi.org/10.1029/2018JC014775).

Rayner, N., Parker, D. E., Horton, E., Folland, C., Alexander, L., Rowell, D., Kent, E., and Kaplan, A. Global analyses of sea surface temperature, sea ice, and night marine air temperature since the late nineteenth century. *Journal of Geophysical Research: Atmospheres*, 108(D14), 2003. doi: [10.1029/2002JD002670](https://doi.org/10.1029/2002JD002670).

Redi, M. H. Oceanic Isopycnal Mixing by Coordinate Rotation. *Journal of Physical Oceanography*, 12(10):1154–1158, 1982. doi: [10.1175/1520-0485\(1982\)012;1154:OIMBCR;2.0.CO;2](https://doi.org/10.1175/1520-0485(1982)012;1154:OIMBCR;2.0.CO;2).

Rignot, E., Mouginot, J., Scheuchl, B., van den Broeke, M., van Wessem, M. J., and Morlighem, M. Four decades of Antarctic Ice Sheet mass balance from 1979–2017. *Proceedings of the National Academy of Sciences*, 116(4):1095–1103, 2019. doi: [10.1073/pnas.1812883116](https://doi.org/10.1073/pnas.1812883116).

Roemmich, D. and Gilson, J. The global ocean imprint of ENSO. *Geophysical Research Letters*, 38(13), 2011. doi: [10.1029/2011GL047992](https://doi.org/10.1029/2011GL047992).

Scott Yiu, Y. Y. and Maycock, A. C. On the Seasonality of the El Niño Teleconnection to the Amundsen Sea Region. *Journal of Climate*, 32(15):4829–4845, 2019. doi: [10.1175/JCLI-D-18-0813.1](https://doi.org/10.1175/JCLI-D-18-0813.1).

Shi, J.-R., Xie, S.-P., and Talley, L. D. Evolving Relative Importance of the Southern Ocean and North Atlantic in Anthropogenic Ocean Heat Uptake. *Journal of Climate*, 31(18):7459–7479, 2018a. doi: [10.1175/JCLI-D-18-0170.1](https://doi.org/10.1175/JCLI-D-18-0170.1).

Shi, J.-R., Xie, S.-P., and Talley, L. D. Evolving relative importance of the southern ocean and north atlantic in anthropogenic ocean heat uptake. *Journal of Climate*, 31(18):7459–7479, 2018b. doi: [10.1175/JCLI-D-18-0170.1](https://doi.org/10.1175/JCLI-D-18-0170.1).

Spence, P., Griffies, S. M., England, M. H., Hogg, A. M., Saenko, O. A., and Jourdain, N. C. Rapid subsurface warming and circulation changes of Antarctic coastal waters by poleward shifting winds. *Geophysical Research Letters*, 41(13):4601–4610, 2014. doi: [10.1002/2014GL060613](https://doi.org/10.1002/2014GL060613).

Spence, P., Holmes, R. M., Hogg, A. M., Griffies, S. M., Stewart, K. D., and England, M. H. Localized rapid warming of West Antarctic subsurface waters by remote winds. *Nature Climate Change*, 7(8):595, 2017. doi: [10.1038/nclimate3335](https://doi.org/10.1038/nclimate3335).

Stammerjohn, S. E., Martinson, D. G., Smith, R. C., Yuan, X., and Rind, D. Trends in Antarctic annual sea ice retreat and advance and their relation to El Niño/Southern Oscillation and Southern Annular Mode variability. *Journal of Geophysical Research: Oceans*, 113(C3), 2008. doi: [10.1029/2007JC004269](https://doi.org/10.1029/2007JC004269).

Stewart, K., Hogg, A. M., Griffies, S., Heerdegen, A., Ward, M., Spence, P., and England, M. Vertical resolution of baroclinic modes in global ocean models. *Ocean Modelling*, 113:50–65, 2017. doi: [10.1016/j.ocemod.2017.03.012](https://doi.org/10.1016/j.ocemod.2017.03.012).

Thompson, A. F., Heywood, K. J., Schmidtko, S., and Stewart, A. L. Eddy transport as a key component of the Antarctic overturning circulation. *Nature Geoscience*, 7(12):879–884, 2014. doi: [10.1038/ngeo2289](https://doi.org/10.1038/ngeo2289).

Timmermann, A., An, S.-I., Kug, J.-S., Jin, F.-F., Cai, W., Capotondi, A., Cobb, K., Lengaigne, M., McPhaden, M. J., Stuecker, M. F., Stein, K., Wittenberg, A. T., Yun, K.-S., Bayr, T., Chen, H.-C., Chikamoto, Y., Dewitte, B., Dommenget, D., Grothe,

P., Guilyardi, E., Ham, Y.-G., Hayashi, M., Ineson, S., Kang, D., Kim, S., Kim, W., Lee, J.-Y., Li, T., Luo, J.-J., McGregor, S., Planton, Y., Power, S., Rashid, H., Ren, H.-L., Santoso, A., Takahashi, K., Todd, A., Wang, G., Wang, G., Xie, R., Yang, W.-H., Yeh, S.-W., Yoon, J., Zeller, E., and Zhang, X. El Niño–Southern Oscillation complexity. *Nature*, 559(7715):535–545, 2018. doi: [10.1038/s41586-018-0252-6](https://doi.org/10.1038/s41586-018-0252-6).

Tsujino, H., Urakawa, S., Nakano, H., Small, R. J., Kim, W. M., Yeager, S. G., Danabasoglu, G., Suzuki, T., Bamber, J. L., Bentsen, M., et al. JRA-55 based surface dataset for driving ocean–sea-ice models (JRA55-do). *Ocean Modelling*, 130:79–139, 2018. doi: [10.1016/j.ocemod.2018.07.002](https://doi.org/10.1016/j.ocemod.2018.07.002).